

pubs.acs.org/JPCC Article

Methylisatin Structural Isomers Have Different Kinetic Pathways to Self-Assembly

Angela M. Silski-Devlin, Jacob P. Petersen, Jonathan Liu, Steven A. Corcelli, and S. Alex Kandel*



Cite This: J. Phys. Chem. C 2020, 124, 17717-17725



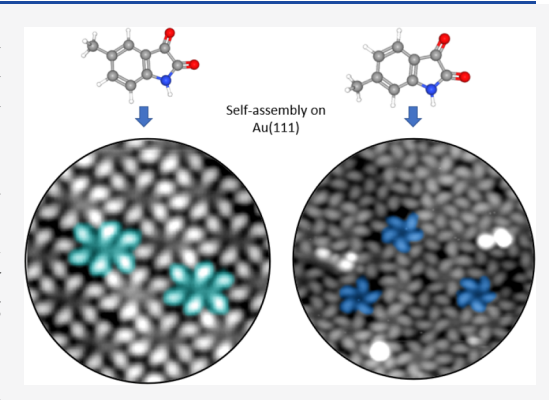
ACCESS

Metrics & More



Supporting Information

ABSTRACT: Monolayers of methylisatin structural isomers are prepared on the Au(111) surface and imaged using scanning tunneling microscopy in ultrahigh vacuum. Monolayer preparation via solution deposition results in different monolayer structures for these two isomers. 5-Methylisatin forms rectangular hexamer clusters that are closely packed, while 6-methylisatin forms cyclic pentamers, dimers, and a close-packed phase. Monolayer preparation via vapor deposition results in the formation of cyclic pentamers for both 5- and 6-methylisatin. These results are compared to isatin monolayers, which also form cyclic pentamers upon both solution and vapor deposition. DFT binding energy calculations corroborate a stable pentamer, as there is a calculated binding energy well for 5-molecule clusters for isatin, 5-methylisatin, 6-methylisatin. The formation of the unusual 5-methylisatin hexamer structure is likely due to nonequilibrium adsorption kinetics present in the solution (pulse) deposition preparation technique.



■ INTRODUCTION

Molecular self-assembly is the process by which disordered molecules spontaneously associate under the influence of noncovalent interactions into extended, ordered structures. There are many fundamental questions of interest in the field of molecular self-assembly, including how molecules self-assemble into a particular structural motif, why some molecules self-assemble into a range of different structures, and how the formation of these structures can be predicted and controlled.

The prediction of crystal structures *a priori*, given only the structure of the starting molecule, is a difficult task, ^{2,3} especially when there are multiple hydrogen-bond-capable functional groups on the starting molecule.⁴ Current crystal structure prediction methods often ignore templating or other kinetic factors, which can result in the formation of various polymorphs.^{5,6} To realize control over crystal polymorph formation and controlled materials design, a greater understanding of the noncovalent interactions that drive structure formation is needed, in addition to the kinetic factors (temperature, concentration, rate of deposition) that direct crystallization pathways. Development of this fundamental understanding will have important implications in crystal engineering, crystal polymorphism, and organic electronics, where the changes in structure can lead to changes in properties of the device/material.^{7–9}

There is great interest in gaining an understanding of how small changes in molecular structure, including position of functional groups^{10–12} and molecular geometry, ^{13–15} lead to changes in self-assembled structure. Forging this connection

between molecular structure and extended structure is not trivial, especially since one molecule may form multiple different 2D morphologies, 16,17 and structural isomers may exhibit vastly different self-assembled structures. 10,12,15,18 In this work, our focus is on self-assembly in two dimensions (which is essentially a simplified process of crystallization with reduced dimensionality) at the vacuum-solid interface. We systematically vary sample preparation conditions as well as alter the functional groups of the starting molecule to demonstrate which factors drive the formation of particular two-dimensional assemblies. In addition, we are interested in self-assembly of molecules in solution and compare solutionstate behavior to their two-dimensional organization. The selfaggregation of molecules in solution is of particular interest in the studies of crystallization mechanisms, as the presence of stable clusters prior to nucleation of crystal growth (prenucleation clusters) has challenged the long-standing classical nucleation theory of crystal formation. 19-2

Previous work from our laboratory has demonstrated that metastable cyclic pentamers of isatin form on the Au(111) surface; these pentamers are stabilized by NH···O hydrogen bonds in addition to a secondary weak CH···O hydrogen

Received: June 16, 2020 Revised: July 20, 2020 Published: July 21, 2020





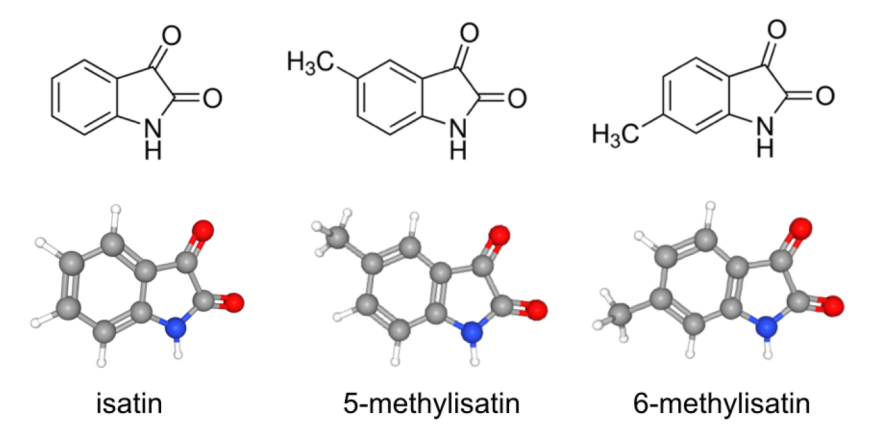


Figure 1. Structures of the molecules discussed in this study.

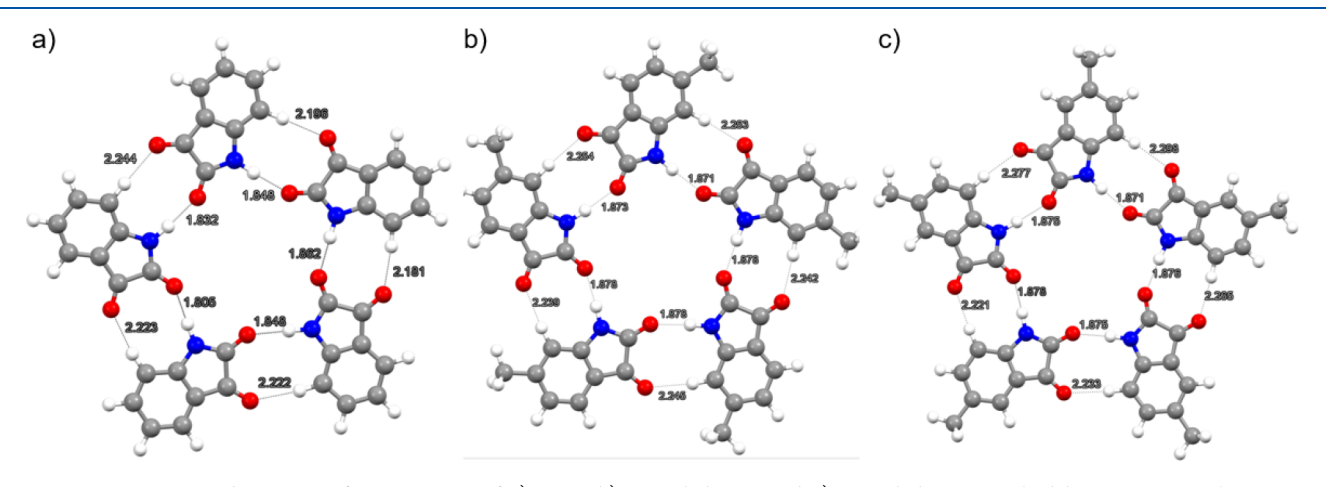


Figure 2. DFT optimized geometry for pentamers of a) isatin b) 6-methylisatin and c) 5-methylisatin. Dashed lines represent the proposed hydrogen bond contacts and the H···A calculated distances in Ångstroms are included.

bond.²² The current study is of methylated isatin derivatives that are functionalized at the 5 and 6 positions, which are remote from the hydrogen bond contacts that form the isatin pentamer (structures shown in Figure 1). The substitution of a methyl group was chosen to test the effect of a non-hydrogen-bonding functional group on the formation of the cyclic pentamers. The surprising result is that the 5- and 6-methylisatin structural isomers form different self-assembled monolayer morphologies on the Au(111) surface as a result of solution deposition; however, as a result of vapor deposition, all three molecules form cyclic pentamers. It is likely that the adsorption kinetics of the nonequilibrium solution deposition process play a significant role in the formation of the 5-methylisatin hexamer. We show that structural isomers 5- and 6-methylisatin have different kinetic pathways to self-assembly.

METHODS

Scanning Tunneling Microscopy. Au(111)-on-mica substrates were cleaned in high vacuum with two cycles of Ar⁺ sputtering (0.55 kV for 15 min) and annealing at 350–400 °C. Substrates were allowed to cool before being transfered to a load-lock chamber for preparation of the monolayer. 6-Methylisatin (6-methyl isatinic anhydride) and 5-methylisatin were purchased from Sigma-Aldrich and used without further purification. For pulsed deposition, solutions with a concentration of 5 mM were prepared in methanol. Droplets of solutions of the molecule of interest were delivered to the surface via a pulsed-solenoid valve (Parker Instruments, Series

9, Iota One Driver, 0.5 mm diameter nozzle) onto the cleaned Au(111) substrate kept at room temperature in a load-lock chamber. For vapor-deposited samples, the gold substrate was exposed to vapor pressure of the methylisatin from a quartz crucible heated to 40–50 °C for 1 min. For either sample preparation method, the sample was then transferred to an Omicron LT-STM, kept at a base pressure of 5 \times 10 $^{-10}$ Torr, and was cooled to 77 K. All images were acquired with a Pt/Ir tip in constant current mode with a tunneling current of 10 pA and a tip—sample bias of +1.0 V, unless otherwise noted.

Electrospray Ionization Mass Spectrometry. Electrospray ionization mass spectrometry (ESI–MS) experiments were done using a Waters Acquity tandem triple quadrupole equipped with a ZSpray electrospray ionization source. Solvated analyte solutions were injected into the electrospray capillary via a syringe pump (Harvard Scientific) at a flow rate of 10 μ L/min. Spectra were collected in positive ion mode. The electrospray source conditions were chosen to maximize ion transmission and to minimize the dissociation of molecular cluster ions. The electrospray parameters were as follows: capillary voltage = 4.0 kV, cone voltage = 10–20 V, source temperature = 50 °C, desolvation temperature = 50 °C. Individual scan time was typically 3 s; spectra were acquired for 3 min

Density Functional Theory. All calculations were performed with the Q-Chem 5.0 software package.²³ As in our previous studies on this class of molecules,²² all structures were optimized using the B3LYP exchange-correlation func-

tional, along with the 6-311++G(d,p) basis set and Grimme's D3 dispersion correction. The initial geometries of the multimolecular structures were generated to be cyclic n-mers, where n is the number of molecules in the cluster. All structures were started in a planar geometry and subjected to the Boys and Bernardi counterpoise correction to account for basis set superposition error. ²⁵

Geometry optimization of the five-molecule clusters of the methylated species resulted in a loss of C_5 symmetry. To rectify this, the first optimized structure was used to determine an average N–H···O bond distance, and a C_5 -symmetric structure with this N–H···O bond distance was used as the starting structure for a second optimization step. This second step was performed with two atoms on each molecule, the nitrogen and the 7-position hydrogen, fixed in three dimensions to ensure the structures would retain C_5 symmetry through the optimization process. The per-molecule binding energy difference between C_5 -symmetric and asymmetric optimized clusters was no more than 0.6 kJ/mol

RESULTS AND DISCUSSION

DFT Optimized Geometries and Binding Energies. Figure 2 shows the optimized DFT-calculated geometries for a cyclic pentamer of isatin and the methyl-substituted isatins. The pentamer of isatin is C₅ symmetric, while 5- and 6methylisatin diverged from C₅ symmetry. DFT calculates short NH···O and CH···O hydrogen bonds for isatin and the methylisatin derivatives. The H···A distances calculated for the CH···O hydrogen bonds for these three molecules are relatively short; weak hydrogen bonds are generally considered to have an H···A distance of 2.2-3.0 Å. 26 Previously, we show experimentally that pentamer formation is precluded when chemical susbtitutions to isatin are made which disrupt the NH···O and CH···O hydrogen bond formation. 15,22 Figures 2b, c show that the substitution of a methyl group remote to these hydrogen bond contacts does not significantly alter the geometry of the pentamer; that is, the 7-position proton and the 3-position carbonyl group are still in close enough proximity to feasibly hydrogen bond.

Optimized minimum-energy structures in the gas-phase of dimers through pentamers for isatin and 5- and 6-methylisatin were calculated using density functional theory. The permolecule binding energies for the these clusters are plotted as a function of number of molecules, n, per cluster and are displayed in Figure 3. The expected trend might be that as the number of molecules in a cluster increases, the per-molecule binding energy of the cluster would increase due to energetically unfavorable steric hindrance associated with increasing the number of molecules in close proximity. However, as Figure 3 shows, the binding energy for these molecular clusters becomes more favorable as n increases from 2 to 5, where the pentamer is 18.5, 16.0, and 16.8 kJ/mol more favorable than the dimer for 6-methylisatin, 5-methylisatin, and isatin, respectively. In our previous study of isatin, we had attributed this decrease in binding energy with increasing cluster size to the formation of an additional weak CH···O hydrogen bond, in which the distance between the 7-position aromatic proton (H-bond donor) and the 3-position carbonyl group (H-bond acceptor) is decreased with more molecules in the cluster, up to n = 5. The additional weak hydrogen bond provides stabilization to the cluster that is greater than the energetically unfavorable steric interactions. It is unsurprising that the methylated isatins follow the same trend in per-

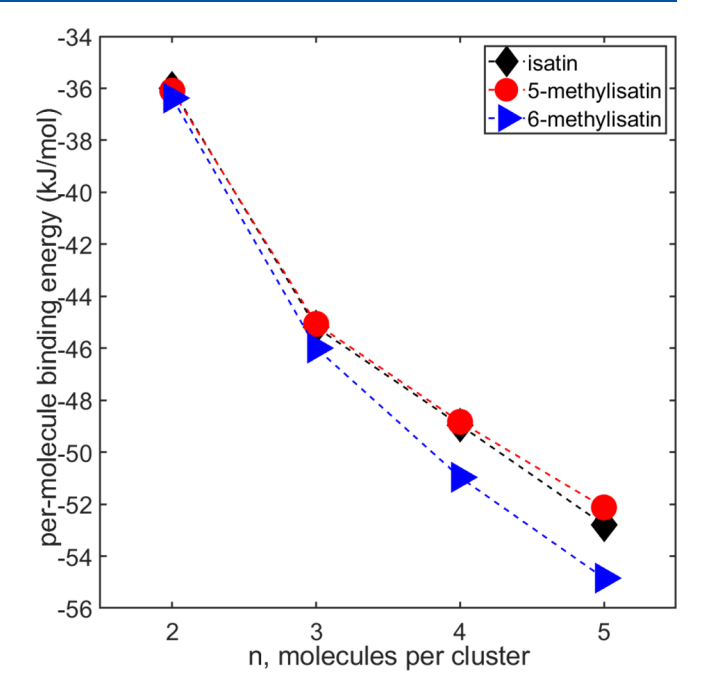


Figure 3. Plot of DFT-calculated per-molecule binding energies as a function of *n*, number of clusters in a cluster of isatin, 5-methylisatin, and 6-methylisatin. All three molecules exhibit the same anomalous trend in decreasing per-molecule binding energy with increasing number of molecules in a cluster.

molecule binding energy vs n as isatin, given that the methylisatin derivatives would, in principle, still be able to form the same hydrogen-bonded contacts as isatin.

Scanning Tunneling Microscopy Data. Figure 4 shows a variety of structural phases of 6-methylisatin that form as a result of pulse deposition on the Au(111) surface. In Figure 4a, cyclic pentamers of 6-methylisatin are observed on the surface. This was the prediction of our model for the cyclic pentamer of isatin: the methyl group is remote from hydrogen bonding and thus should not affect pentamer formation. Figures 4b, c show two additional phases: dimer rows and close packing of molecules. This is in contrast to the isatin monolayers that we previously observed that consisted of exclusively cyclic pentamers.²² The presence of multiple structural phases on the 6-methylisatin monolayer could potentially arise from either thermodynamic or kinetic factors. One possibility is that 6-methylisatin pentamers are destabilized on the surface relative to other packing geometries; alternately, the barriers to formation of these various structures may be altered by methylation.

The structural isomer 5-methylisatin, pulse deposited on Au(111), results in a monolayer structure that is structurally dissimilar to that of either 6-methylisatin or isatin. Figures 5a, b show that monolayers of 5-methylisatin consist of close-packed rectangular hexamers. The fast Fourier transform (Figure 5b inset) shows that the hexamers on the surface pack with periodic order. Figure 5a shows that the hexamers arrange around vacancies, and Figure S1 shows hexamers at an edge of the ordered area; these observations further confirm that the hexamers shown are the repeating unit for this monolayer.

Upon thermal annealing, the 5-methylisatin hexamers reorganize into dimer rows (Figure S2), which indicates that the hexamer is a metastable intermediate structure. It is a surprising result that the 5- and 6-methylisatin molecules have

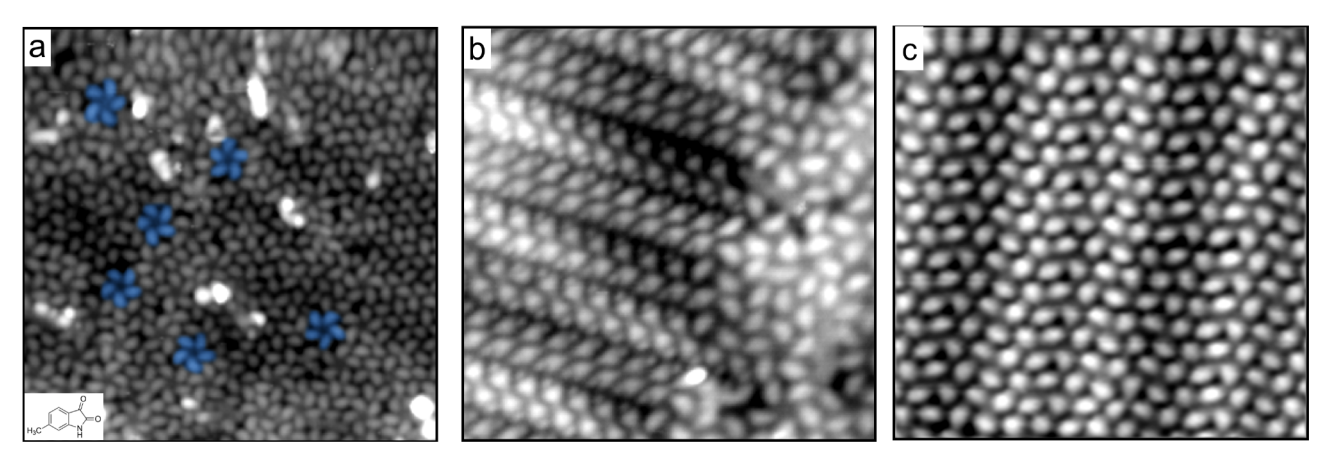


Figure 4. STM images of pulse deposited 6-methylisatin on Au(111). (a) A 200 × 200 Å area of pentamer clusters (representative clusters highlighted in blue). (b) An area of chains of dimers, 109 × 109 Å. (c) Close-packed phase of molecules, 120 × 120 Å.

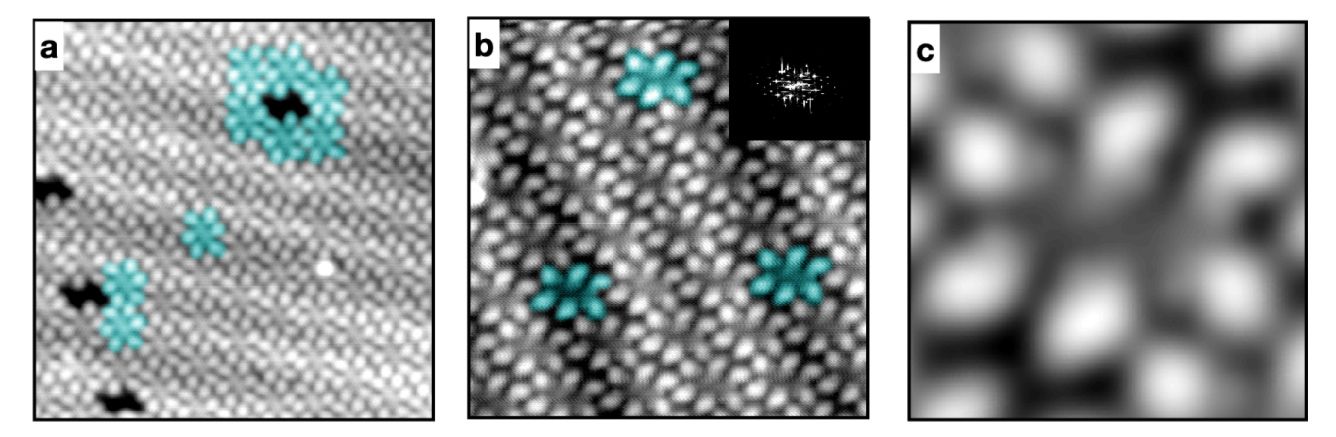


Figure 5. STM images of 5-methylisatin pulse deposited on Au(111). Representative hexamers are highlighted in light blue. (a) A 180×180 Å area and (b) A 120×120 Å area, tunneling current = 0.02 nA, $V_{\rm B}$ = +1.0 V. Inset: fast Fourier transform of the area shown in panel b. (c) Composite image of 67 hexamers (23 × 23 Å).

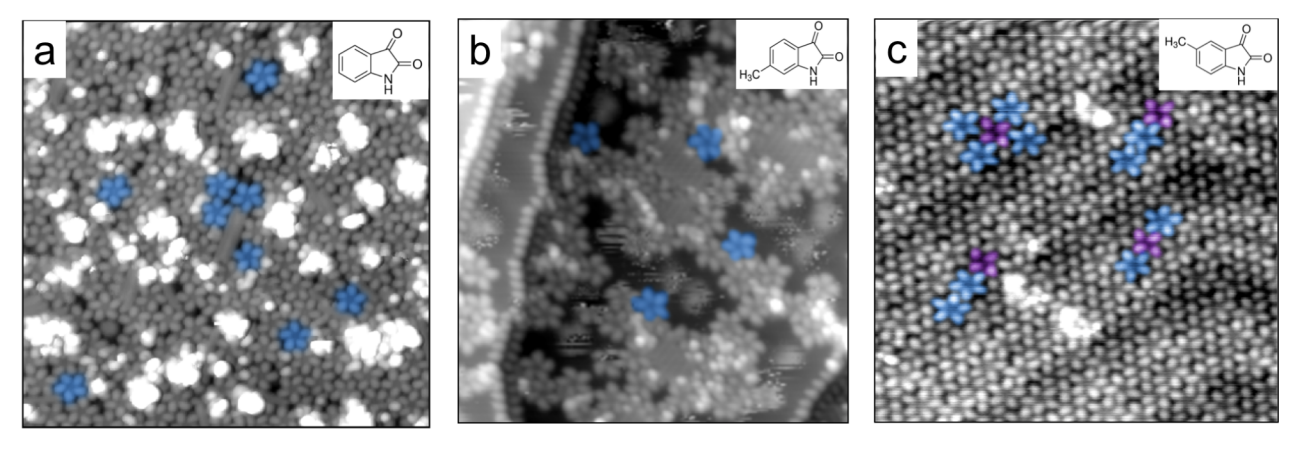


Figure 6. STM images of vapor-deposited monolayers on the Au(111) surface. Representative pentamer structures are highlighted in blue. (a) Isatin ($250 \times 250 \text{ Å}$), (b) 6-methylisatin ($250 \times 250 \text{ Å}$), and (c) 5-methylisatin pentamers with intercalated tetramers colored in purple ($200 \times 200 \text{ Å}$).

such different monolayer structures, especially given the molecules' similar trends in per-molecule binding energy as a function of number of molecules in the cluster (Figure 3). While it has been observed that moving an alkyl group by one position can result in different 2D morphologies, ^{10,12,27} this is typically due to the difference in van der Waals forces that result from interactions between bulky alkyl chains. A methyl group, the shortest alkyl chain, would not be expected to

engage in any significant van der Waals interactions that would drive self-assembly.

The monolayer preparation method of pulse deposition is traditionally used to deliver molecules to the surface that would not survive the heating required to sublime the molecule on the surface (which is the typical method of monolayer preparation in UHV) such as DNA, 28 π -conjugated oligomers, 29,30 fullerenes, 31 and polymers. 32 It has been

observed for indole-2-carboxylic acid (a small organic molecule) that metastable clusters form via pulse deposition, ³³ whereas a monolayer of the same molecule prepared via vapor deposition resulted in catemers, a motif reminiscent of the solid-state crystal structure. ³⁴ This vast difference in monolayer composition for the same molecule was rationalized by the nonequilibrium adsorption kinetics that are present in the solution deposition process. According to Ostwald's rule, crystallization from a solution or a melt will result in the formation of the least stable polymorph first. ³⁵ Given that the small organic molecules in this study would likely remain intact upon heating, we also performed vapor deposition experiments of isatin and the methyl-substituted derivatives to determine whether these unusual morphologies are dependent on the nonequilibrium adsorption kinetics in pulse deposition.

Figure 6 includes STM images of vapor deposited monolayers of isatin, 5-methylisatin, and 6-methylisatin on the Au(111) surface. The monolayers of isatin and the methylisatin derivatives all consist of cyclic pentamers. While we had expected these three molecules to form pentamers via pulse deposition, this was the first time that our laboratory has observed pentamers upon vapor deposition of the same molecule. While monolayers of 6-methylisatin were mixed with pentamers and dimer chains (Figure S4), it was unexpected to observe pentamers of 6-methylisatin at a relatively low surface coverage (Figure 6b).

Barth and coworkers suggest a model that describes the kinetics and thermodynamics of surface growth processes that involve the rate of deposition compared to the rate of diffusion of molecules on the surface.³⁶ In this model, they propose that monolayers with a low rate of deposition relative to diffusion will result in thermodynamic surface growth, whereas a high rate of deposition relative to diffusion will result in kinetic trapping of molecules on the surface. Typically, the pulse deposition process is associated with kinetically controlled monolayer growth, while vapor deposition often results in thermodynamic monolayer growth. For the case of indole-2carboxylic acid, pentamers, hexamers, and catemers were present on the pulse-deposited monolayer,³³ whereas the vapor-deposited monolayer consisted of purely catemers, which is the structural motif reminiscent of the crystal structure.³⁴ Isatin pentamers reorganized into dimers upon thermal annealing, 22 suggesting that the pentamer configuration is a local energy-minimum energy structure, while the dimer configuration is the global minimum. For all three molecules to form unusual cyclic pentamers upon vapor deposition further points to the anomalous stability of a pentamer.

In addition, the 5-methylisatin monolayer structure that consists of pentamers (Figure 6c) is different as a result of the two preparation methods; this molecule formed close-packed hexamers upon pulse deposition (Figure 5). There are additional structural phases that were resolved on the monolayer of vapor-deposited 5-methylisatin (Figure S3). Nonetheless, 5-methylisatin hexamers were completely absent from the vapor-deposited monolayer. The absence of the 5-methylisatin hexamers on the vapor-deposited monolayer suggests that the nonequilibrium adsorption kinetics of pulse deposition provides access to unique structures that do not form closer to equilibrium. While all three molecules have unusual stability associated with 5-molecules in a cluster, we observe that 5-methylisatin has a different kinetic pathway to

pentamer formation, with hexamers as a kinetically locked intermediate structure.

The 5-methylisatin vapor-deposited monolayer is also notable because of its tight packing of pentamers with what appear to be intercalated tetramers (shown in purple in Figure 6c). In Figure 7, 5-methylisatin pentamers are outlined with





Figure 7. STM images of densely packed pentamers of 5-methylisatin and measured orientational distributions of the pentamers. Pentamers are outlined in pentagons, and the colors of the pentagons correspond to the directions of the pentamer's symmetry axis. The tick marks on the color wheel show the orientation of each pentamer. The distribution of angles is peaked around two angles. Inset: fast Fourier transform of the image.

pentagons with a color that corresponds to the direction of the pentamer's orientation. The angular distributions of the pentamers are peaked around two angles, as illustrated by the blue and orange pentagons outlining the pentamers. The pentamers of a given orientational angle are lined up in rows, and in between neighboring rows there are extra molecules, which appear to be tetramers. This close packing of pentamers with two sharp angles of orientation is reminiscent of ferrocenecarboxylic acid in which there were intercalated dimers in between pentamers.³⁷ The fast Fourier transform of this monolayer is shown in the inset of Figure 7, which corroborates the periodic order of the pentamer orientations. This ordered angular distribution of pentamers suggests that there are pentamer-pentamer noncovalent interactions that drive the close packing of these pentamers. The periodic order of 5-methylisatin pentamers and intercalated tetramers is in contrast to the pentamers of isatin, which do not exhibit any orientational order (Figure S5).

Another interesting feature to note in Figure 7 is that the direction of the pentamer packing (as visualized with orange and blue pentagons) is not aligned along the Au(111) herringbone reconstruction; rather, pentamers appear to be oriented perpendicular to the Au(111) herringbone reconstruction. The herringbone reconstruction is a feature of the Au(111) surface that arises due to the lack of coordination of the surface layer compared to the bulk layers, resulting in a contraction of Au atoms on the surface layer³⁸ which is resolved in our images (Figures 6c and 7) as "herringbone" rows of periodic change in contrast. Perturbations in the periodicity of the herringbone reconstruction are a good

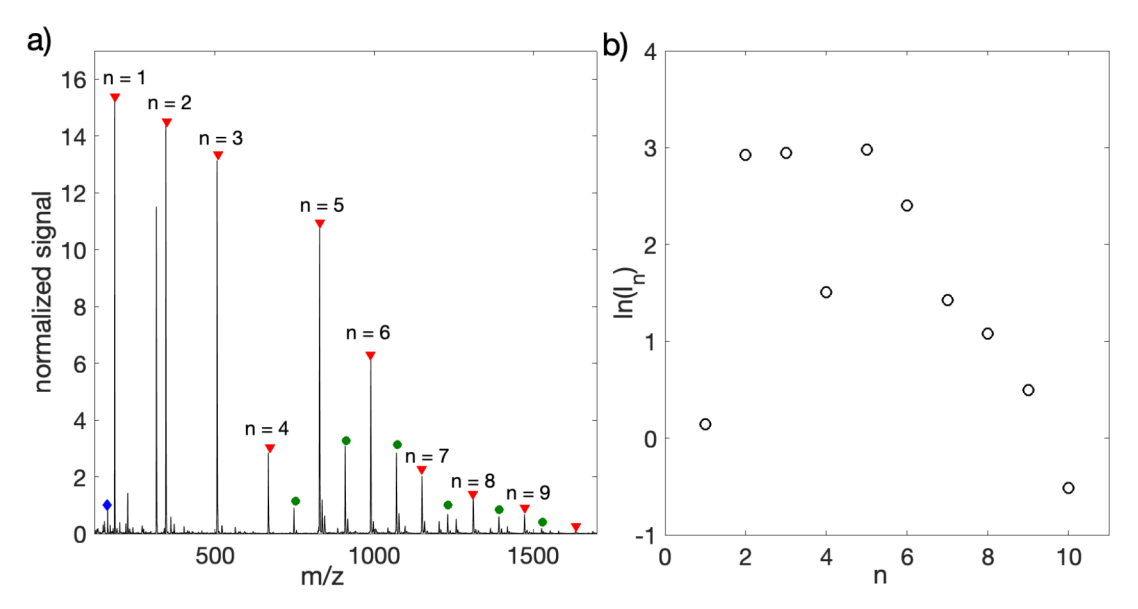


Figure 8. (a) A positive ion mode mass spectrum of 6-methylisatin 5 mM in acetonitrile. Capillary voltage = 4.25 kV and cone voltage = 30 V. $[M_n+2N_a]^{+2}$ peaks for odd numbered n for n=9-19 are indicated in the spectrum with a green circle. $[M_n+N_a]^+$ peaks for n=1-10 are indicated by a red triangle. (b) Log plot of integrated peak intensity as a function number of molecules per cluster, n, for all singly charged clusters.

indicator of molecule—surface interaction strength.^{39,40} Caffeine, a structurally similar molecule to the molecules in the present study, was shown to have weak interactions with the Au(111) surface as demonstrated by no structural changes to the herringbone reconstruction.⁴¹ Here, we suggest that 5-methylisatin does not strongly interact with the underlying gold surface, given no structural change to the herringbone reconstruction. However, the observation that the rows of 5-methylisatin pentamers pack perpendicular to the herringbone suggests that the underlying gold surface may influence orientational packing of the monolayer structure.

Electrospray Ionization Mass Spectrometry Data. Electrospray ionization (ESI) is a gentle method of ionization that does not fragment the molecule and maintains noncovalent interactions upon ionization. 42,43 The most common use of ESI is for the study of large biomolecules, because the soft ionization technique (and the presence of multiply charged ions) allows proteins to remain intact, and thus structural and amino acid sequence information can be obtained.44 ESI is not limited to the study of proteins, however. It has been shown to be effective for the study of small organic molecules⁴⁵ organometallic compounds,⁴⁶ metal—organic complexes,⁴⁷ and in supramolecular chemistry. 48 Our group has previously exploited ESI-MS of small organic compounds in conjunction with STM to observe the noncovalent clustering of these molecules to elucidate the mechanism of formation of the surface-bound clusters, 22,49,50 that is, to answer the question of whether clusters are forming in solution or if they diffuse and reorganize on the surface into the clusters that we image via STM.

A mass spectrum of 6-methylisatin is plotted in Figure 8a. The most intense peak in each family of peaks is the $[M_n+Na]^+$ peak, which is observed for n=1-9. In addition, $[M_n+2Na]^{+2}$ peaks are observed in the spectrum for odd-numbered clusters for n=9-19 (and presumably are also present for even-number clusters, underneath the $[M_n+Na]^+$ peaks). An interesting feature shown in Figure 8 is the anomalous intensity of the $[M_5+Na]^+$ peak $(827 \ m/z)$ relative to the

tetramer peak $[M_4+Na]^+$ peak (645 m/z), where the pentamer peak is roughly 4 times more intense than the tetramer peak.

This observation goes against the expectation of an exponential decay of signal intensity as a function of the number of molecules per cluster. A similar n=4 vs n=5 anomaly was also observed for isatin. One explanation is that n=5 is a "magic number", reflecting an unusual stability associated with 5-molecule gas-phase ion clusters; this would be in line with our STM results, where pentamers are a common feature. Alternately, the data could be interpreted as showing an "antimagic number" cluster for n=4, with an anomalous instability for clusters of this size. This would be an unusual result, as antimagic clusters are typically observed for larger clusters that can fragment into magic-number clusters. $^{51-53}$

In addition, there are relatively intense $[M_n+2Na]^{+2}$ peaks for n=9,11,13, while we do not observe clusters of this size in our STM images. One possibility is that these large clusters could consist of pentameric clusters, with additional 6-methylisatin molecules attached to the pentamers. It is also likely that while these high-n oligomer structures may be stable as gas-phase ions, the surface-supported structures for these oligomers are not stable in 2D adsorption geometries.

While it is not obvious that gas-phase ionic clusters produced via ESI are directly comparable to the neutral surface-adsorbed molecular clusters that we image on a surface, the greater relative intensity of 6-methylisatin pentamers in a mass spectrum suggest that a surface is not critical for the stabilization of 5-molecule clusters. Rather, these unusual 5molecule clusters can form as gas-phase ions (and possibly in solution) in addition to on a surface. Alternative to the clusters forming in solution, the clusters may form due to the nonequilibrium conditions that the solution is exposed to upon electrospray ionization. Upon solvent evaporation, the volume of the droplet decreases, which results in a superconcentrated droplet⁵⁴ which may result in anomalous intensities of higher-n oligomer gas-phase ions. Other factors such as temperature changes in the droplets^{54,55} are kinetic factors that occur in electrospray ionization that may cause the

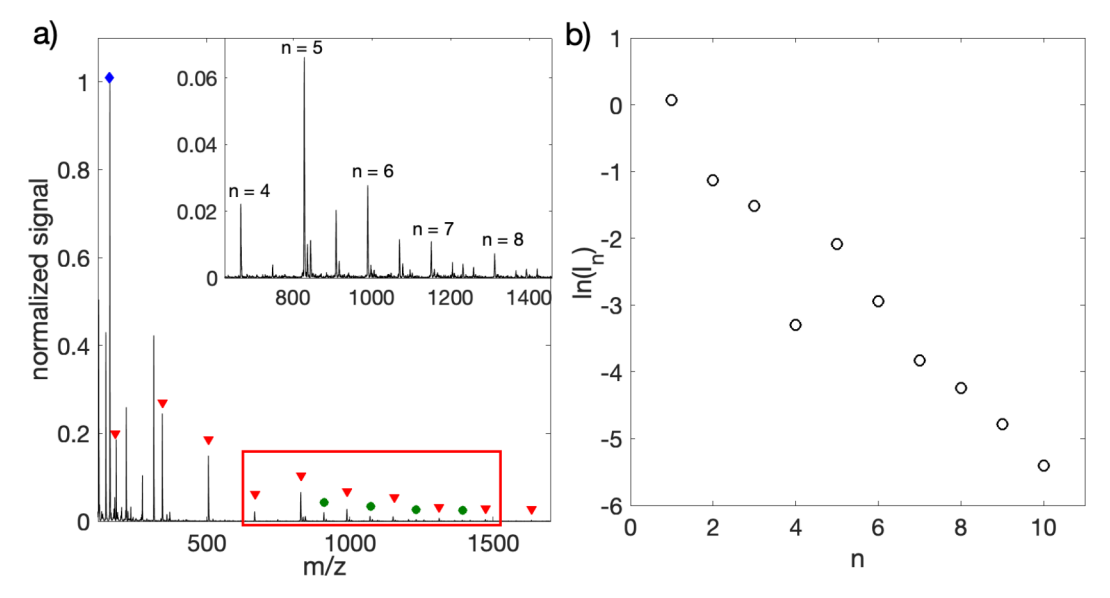


Figure 9. (a) A positive ion mode mass spectrum of 5-methylisatin, 5 mM in acetonitrile. Capillary voltage = 4.25 kV and cone voltage = 30 V. Signal is normalized to the protonated monomer peak. $[M_n+2Na]^{+2}$ peaks for odd numbered n for n=9-19 are indicated in the spectrum with a green circle. Inset: zoomed in spectrum in the region $600-1500 \ m/z$, with the $[M_n+Na]^+$ peak shown for n=4-8. The $[M_n+H]^+$ peak is indicated by a blue diamond, and $[M_n+Na]^+$ peaks for n=1-10 are indicated by a red triangle. Unlabeled peaks were present in the background spectrum. (b) Log plot of integrated peak intensity as a function number of molecules per cluster, n.

formation of gas-phase ions that may not be representative of the solution chemistry. Our monolayer preparation technique (pulsed deposition) is also a process that involves the rapid evaporation of solvent in vacuum, so potentially electrospray ionization and pulsed deposition result in analogous nonequilibrium processes.

A typical ESI mass spectrum for a 5 mM solution of 5methylisatin in acetonitrile is plotted in Figure 9a. In this spectrum, the [M₁+H]⁺ (protonated monomer) peak is the most intense peak and $[M_n+N_a]^+$ peaks for n=1-10. Doubly charged larger oligomer peaks $([M_n+2Na]^{+2})$ for oddnumbered n where n = 9-19 are also present in the spectrum in between the singly charged peaks. The log plot shown in Figure 9b displays the nonlinear trend of signal intensity with increasing *n*. While the log plot of 5-methylisatin is more linear than the log plot of 6-methylisatin (Figure 8b), the n = 5 peak positively deviates from the linear fit, and n = 4 negatively deviates from the linear fit (Figure S5). Given these intensities of n = 4 and n = 5 peaks for 5-methylisatin, it is difficult to make a statement if the tetramer is anomalously unstable or if the pentamer is anomalously stable (or both), as discussed previously for 6-methylisatin. Regardless, in the relatively low intensity of n = 4 clusters compared to n = 5 and higher-nclusters, there is a marked similarity between 5-methylisatin and 6-methylisatin, and both are in line with previous observations of isatin.²²

The agreement of an anomalously intense pentamer peak in the mass spectra of isatin, 5-methylisatin, and 6-methylisatin corroborate the finding that pentamers form on a vapor-deposited monolayer for each of these molecules. There does not appear to be an intense hexamer peak in the mass spectrum of 5-methylisatin; however, a pulse-deposited monolayer of 5-methylisatin consisted of hexamers (Figure 5). The absence of an unusually intense hexamer peak in the mass spectrum of 5-methylisatin may indicate that hexamers of 5-methylisatin are kinetically locked on the surface but are not present in rapidly evaporating droplets.

CONCLUSION

In summary, we investigated the role of the position of a nonhydrogen-bonding methyl group on the self-assembly of isatins on the surface and as aerosolized droplets. We have presented a combined STM, ESI-MS, and DFT investigation of isatin, 5methylisatin, and 6-methylisatin. Isatin forms cyclic pentamers on the Au(111) surface that are supported by NH···O and CH···O hydrogen bonds. 5- and 6-Methylisatin derivatives were examined to determine how a methyl group in a position remote from the isatin pentamer hydrogen-bonding contacts would affect the self-assembled structure. Pulse deposited monolayers of 5-methylisatin consist of ordered networks of rectangular hexamer clusters, whereas 6-methylisatin monolayers consist of dimers, close-packed molecules and pentamers. However, upon vapor deposition, isatin and 5and 6-methylisatin all form cyclic pentamers. While pentamers are a metastable species observed on the Au(111) surface for these 3 molecules, 5-methylisatin has a different kinetic pathway to pentamer formation, with an unusual hexamer structure as an intermediate. The stability of a pentamer is corroborated by a relatively intense pentamer peak in a mass spectrum of isatin and the methylisatin isomers. DFT binding energy calculations support a metastable pentamer structure for all three molecules, as there is a local energy well for a pentamer of each molecule. This work may shed light on the early stages of crystallization and nonclassical prenucleation mechanisms in which molecular clusters are formed in evaporating droplets. In addition, these findings may contribute to the fundamental understanding between molecular structure and supramolecular structure, a question of interest in the fields of crystal engineering and supramolecular chemistry.

ASSOCIATED CONTENT

Supporting Information

The Supporting Information is available free of charge at https://pubs.acs.org/doi/10.1021/acs.jpcc.0c05456.

Additional STM images of as-deposited monolayers, STM images of thermally annealed samples, and residual plot of linear fit of Figure 9b (PDF)

AUTHOR INFORMATION

Corresponding Author

S. Alex Kandel — Department of Chemistry and Biochemistry, University of Notre Dame, Notre Dame, Indiana 46556, United States; Occid.org/0000-0001-8191-1073; Phone: 574-631-7837; Email: skandel@nd.edu

Authors

- **Angela M. Silski-Devlin** Department of Chemistry and Biochemistry, University of Notre Dame, Notre Dame, Indiana 46556, United States
- Jacob P. Petersen Department of Chemistry and Biochemistry, University of Notre Dame, Notre Dame, Indiana 46556, United States
- Jonathan Liu Department of Chemistry and Biochemistry, University of Notre Dame, Notre Dame, Indiana 46556, United States
- Steven A. Corcelli Department of Chemistry and Biochemistry, University of Notre Dame, Notre Dame, Indiana 46556, United States; orcid.org/0000-0001-6451-4447

Complete contact information is available at: https://pubs.acs.org/10.1021/acs.jpcc.0c05456

Notes

The authors declare no competing financial interest.

ACKNOWLEDGMENTS

Support for this work has been provided by the National Science Foundation (NSF Grant CHE-1807313). We would also like to acknowledge the University of Notre Dame Mass Spectrometry Facility for use of instrumentation.

REFERENCES

- (1) Whitesides, G.; Mathias, J.; Seto, C. Molecular self-assembly and nanochemistry: a chemical strategy for the synthesis of nanostructures. *Science* **1991**, *254*, 1312–1319.
- (2) Desiraju, G. R. Crystal engineering: From molecule to crystal. J. Am. Chem. Soc. 2013, 135, 9952–9967.
- (3) Price, S. L. Control and prediction of the organic solid state: a challenge to theory and experiment. *Proc. R. Soc. London, Ser. A* **2018**, 474, 20180351.
- (4) Corpinot, M. K.; Stratford, S. A.; Arhangelskis, M.; Anka-Lufford, J.; Halasz, I.; Judaš, N.; Jones, W.; Bučar, D. K. On the predictability of supramolecular interactions in molecular cocrystals—the view from the bench. *CrystEngComm* **2016**, *18*, 5434—5439.
- (5) Gutzler, R.; Cardenas, L.; Rosei, F. Kinetics and thermodynamics in surface-confined molecular self-assembly. *Chem. Sci.* **2011**, *2*, 2290.
- (6) Hu, Y.; Xu, S.; Miao, K.; Miao, X.; Deng, W. Same building block, but diverse surface-confined self-assemblies: solvent and concentration effects-induced structural diversity towards chirality and achirality. *Phys. Chem. Chem. Phys.* **2018**, 20, 17367–17379.
- (7) Khassanov, A.; Steinrück, H.-G.; Schmaltz, T.; Magerl, A.; Halik, M. Structural investigations of self-assembled monolayers for organic electronics: Results from X-ray reflectivity. *Acc. Chem. Res.* **2015**, *48*, 1901–1908.
- (8) Gentili, D.; Gazzano, M.; Melucci, M.; Jones, D.; Cavallini, M. Polymorphism as an additional functionality of materials for technological applications at surfaces and interfaces. *Chem. Soc. Rev.* **2019**, *48*, 2502–2517.
- (9) Chung, H.; Chen, S.; Sengar, N.; Davies, D. W.; Garbay, G.; Geerts, Y. H.; Clancy, P.; Diao, Y. Single atom substitution alters the

- polymorphic transition mechanism in organic electronic crystals. *Chem. Mater.* **2019**, *31*, 9115–9126.
- (10) Hu, Y.; Miao, K.; Zha, B.; Xu, L.; Miao, X.; Deng, W. STM investigation of structural isomers: alkyl chain position induced self-assembly at the liquid/solid interface. *Phys. Chem. Chem. Phys.* **2016**, *18*, 624–634.
- (11) Brown, R. D.; Corcelli, S. A.; Kandel, S. A. Structural polymorphism as the result of kinetically controlled self-assembly. *Acc. Chem. Res.* **2018**, *51*, 465–474.
- (12) Kikkawa, Y.; Tsuzuki, S.; Kashiwada, A.; Hiratani, K. Selfassembled 2D patterns of structural isomers in isobutenyl compounds revealed by STM at solid/liquid interface. *Colloids Surf., A* **2018**, *537*, 580–590.
- (13) Furukawa, S.; Uji-i, H.; Tahara, K.; Ichikawa, T.; Sonoda, M.; De Schryver, F. C.; Tobe, Y.; De Feyter, S. Molecular Geometry Directed Kagomé and Honeycomb Networks: Toward Two-Dimensional Crystal Engineering. J. Am. Chem. Soc. 2006, 128, 3502—3503.
- (14) Ishikawa, D.; Ito, E.; Han, M.; Hara, M. Effect of the steric molecular structure of azobenzene on the formation of self-assembled monolayers with a photoswitchable surface morphology. *Langmuir* **2013**, *29*, 4622–4631.
- (15) Silski, A. M.; Petersen, J. P.; Brown, R. D.; Corcelli, S. A.; Kandel, S. A. Scanning tunneling microscopy investigation of two-dimensional polymorphism of structural isomers. *J. Phys. Chem. C* **2018**, *122*, 25467–25474.
- (16) Ahn, S.; Matzger, A. J. Six Different Assemblies from One Building Block: Two-Dimensional Crystallization of an Amide Amphiphile. J. Am. Chem. Soc. 2010, 132, 11364–11371.
- (17) Adisoejoso, J.; Tahara, K.; Lei, S.; Szabelski, P.; Rżysko, W.; Inukai, K.; Blunt, M. O.; Tobe, Y.; De Feyter, S. One building block, two different nanoporous self-assembled monolayers: A combined STM and Monte Carlo study. *ACS Nano* **2012**, *6*, 897–903.
- (18) Hu, Y.; Miao, K.; Xu, L.; Zha, B.; Miao, X.; Deng, W. Effects of alkyl chain number and position on 2D self-assemblies. *RSC Adv.* **2017**, *7*, 32391–32398.
- (19) Gebauer, D.; Völkel, A.; Cölfen, H. Stable Prenucleation Calcium Carbonate Clusters. *Science* **2008**, 322, 1819–1822.
- (20) Gebauer, D.; Cölfen, H. Prenucleation clusters and non-classical nucleation. *Nano Today* **2011**, *6*, 564–584.
- (21) Gebauer, D.; Kellermeier, M.; Gale, J. D.; Bergström, L.; Cölfen, H. Pre-nucleation clusters as solute precursors in crystallisation. *Chem. Soc. Rev.* **2014**, *43*, 2348–2371.
- (22) Silski, A. M.; Brown, R. D.; Petersen, J. P.; Coman, J. M.; Turner, D. A.; Smith, Z. M.; Corcelli, S. A.; Poutsma, J. C.; Kandel, S. A. C-H···O hydrogen bonding in pentamers of isatin. *J. Phys. Chem. C* **2017**, *121*, 21520–21526.
- (23) Shao, Y.; Gan, Z.; Epifanovsky, E.; Gilbert, A. T.; Wormit, M.; Kussmann, J.; Lange, A. W.; Behn, A.; Deng, J.; Feng, X.; et al. Advances in molecular quantum chemistry contained in the Q-Chem 4 program package. *Mol. Phys.* **2015**, *113*, 184–215.
- (24) Grimme, S.; Antony, J.; Ehrlich, S.; Krieg, H. A consistent and accurate ab initio parametrization of density functional dispersion correction (DFT-D) for the 94 elements H-Pu. *J. Chem. Phys.* **2010**, 132, 154104.
- (25) Boys, S. F.; Bernardi, F. The calculation of small molecular interactions by the differences of separate total energies. Some procedures with reduced errors. *Mol. Phys.* **2002**, *100*, 65–73.
- (26) Steiner, T. The Hydrogen Bond in the Solid State. *Angew. Chem., Int. Ed.* **2002**, 41, 48–76.
- (27) Kikkawa, Y.; Koyama, E.; Tsuzuki, S.; Fujiwara, K.; Kanesato, M. Bipyridine Derivatives at a Solid/Liquid Interface: Effects of the Number and Length of Peripheral Alkyl Chains. *Langmuir* **2010**, *26*, 3376–3381.
- (28) Tanaka, H.; Kawai, T. Scanning tunneling microscopy imaging and manipulation of DNA oligomer adsorbed on Cu(111) surfaces by a pulse injection method. *J. Vac. Sci. Technol., B: Microelectron. Process. Phenom.* 1997, 15, 602.

- (29) Kasai, H.; Tanaka, H.; Okada, S.; Oikawa, H.; Kawai, T.; Nakanishi, H. STM Observation of Single Molecular Chains of π -Conjugated Polymers. *Chem. Lett.* **2002**, *31*, 696–697.
- (30) Pérez León, C.; Sürgers, C.; Mayor, M.; Marz, M.; Hoffmann, R.; Löhneysen, H. v. STM Investigation of Large π -Conjugated Oligomers and Tetrahydrofuran Codeposited on Cu(111) by Pulse Injection. *J. Phys. Chem. C* **2009**, *113*, 14335–14340.
- (31) Shirai, Y.; Osgood, A. J.; Zhao, Y.; Kelly, K. F.; Tour, J. M. Directional Control in Thermally Driven Single-Molecule Nanocars. *Nano Lett.* **2005**, *5*, 2330–2334.
- (32) Terada, Y.; Choi, B.-K.; Heike, S.; Fujimori, M.; Hashizume, T. Placing Conducting Polymers onto a H-Terminated Si(100) Surface via a Pulse Valve. *Nano Lett.* **2003**, *3*, 527–531.
- (33) Wasio, N. A.; Quardokus, R. C.; Brown, R. D.; Forrest, R. P.; Lent, C. S.; Corcelli, S. A.; Christie, J. A.; Henderson, K. W.; Kandel, S. A. Cyclic hydrogen bonding in indole carboxylic acid clusters. *J. Phys. Chem. C* 2015, *119*, 21011–21017.
- (34) De Marchi, F.; Cui, D.; Lipton-Duffin, J.; Santato, C.; MacLeod, J. M.; Rosei, F. Self-assembly of indole-2-carboxylic acid at graphite and gold surfaces. *J. Chem. Phys.* **2015**, *142*, 101923.
- (35) Threlfall, T. Structural and thermodynamic explanations of Ostwald's Rule. Org. Process Res. Dev. 2003, 7, 1017–1027.
- (36) Barth, J. V.; Costantini, G.; Kern, K. Engineering atomic and molecular nanostructures at surfaces. *Nature* **2005**, 437, 671–679.
- (37) Wasio, N. A.; Quardokus, R. C.; Forrest, R. P.; Lent, C. S.; Corcelli, S. A.; Christie, J. A.; Henderson, K. W.; Kandel, S. A. Selfassembly of hydrogen-bonded two-dimensional quasicrystals. *Nature* **2014**, *507*, 86–90.
- (38) Hanke, F.; Björk, J. Structure and local reactivity of the Au(111) surface reconstruction. *Phys. Rev. B: Condens. Matter Mater. Phys.* **2013**, 87, 235422.
- (39) Rossel, F.; Brodard, P.; Patthey, F.; Richardson, N. V.; Schneider, W.-D. Modified herringbone reconstruction on Au(111) induced by self-assembled Azure A islands. *Surf. Sci.* **2008**, *602*, L115–L117.
- (40) Iski, E. V.; Jewell, A. D.; Tierney, H. L.; Kyriakou, G.; Sykes, E. C. H. Controllable restructuring of a metal substrate: Tuning the surface morphology of gold. *Surf. Sci.* **2012**, *606*, 536–541.
- (41) Schulte, M. G. H.; Jeindl, A.; Baltaci, I.; Roese, P.; Schmitz, M.; Berges, U.; Hofmann, O. T.; Westphal, C. Structural investigation of caffeine monolayers on Au(111). *Phys. Rev. B: Condens. Matter Mater. Phys.* **2020**, *101*, 245414.
- (42) Fenn, J. B.; Mann, M.; Meng, C. K.; Wong, S. F.; Whitehouse, C. M. Electrospray ionization for mass spectrometry of large biomolecules. *Science* **1989**, 246, 64–70.
- (43) Przybylski, M.; Glocker, M. O. Electrospray Mass Spectrometry of Biomacromolecular Complexes with Noncovalent Interactions—New Analytical Perspectives for Supramolecular Chemistry and Molecular Recognition Processes. *Angew. Chem., Int. Ed. Engl.* **1996**, 35, 806–826.
- (44) Domon, B.; Aebersold, R. Mass Spectrometry and Protein Analysis. *Science* **2006**, *312*, 212–217.
- (45) Wilson, S. R.; Wu, Y. Applications of electrospray ionization mass spectrometry to neutral organic molecules including fullerenes. *J. Am. Soc. Mass Spectrom.* **1993**, *4*, 596–603.
- (46) Traeger, J. C. Electrospray mass spectrometry of organometallic compounds. *Int. J. Mass Spectrom.* **2000**, 200, 387–401.
- (47) Keith-Roach, M. J. A review of recent trends in electrospray ionisation-mass spectrometry for the analysis of metal—organic ligand complexes. *Anal. Chim. Acta* **2010**, *678*, 140–148.
- (48) Schalley, C. A. Supramolecular chemistry goes gas phase: the mass spectrometric examination of noncovalent interactions in host—guest chemistry and molecular recognition. *Int. J. Mass Spectrom.* **2000**, 194, 11—39.
- (49) Brown, R. D.; Coman, J. M.; Christie, J. A.; Forrest, R. P.; Lent, C. S.; Corcelli, S. A.; Henderson, K. W.; Kandel, S. A. Evolution of metastable clusters into ordered structures for 1,1'-ferrocenedicarboxylic acid on the Au(111) surface. *J. Phys. Chem. C* **2017**, *121*, 6191–6198.

- (50) Silski-Devlin, A. M.; Petersen, J. P.; Liu, J.; Turner, G. A.; Poutsma, J. C.; Kandel, S. A. Hydrogen-bonded tetramers of carbamazepine. *J. Phys. Chem. C* **2020**, 124, 5213–5219.
- (51) Wei, S.; Shi, Z.; Castleman, A. W. Mixed cluster ions as a structure probe: Experimental evidence for clathrate structure of $(H_2O)_{20}H^+$ and $(H_2O)_{21}H^+$. *J. Chem. Phys.* **1991**, *94*, 3268–3270.
- (52) Fujii, A.; Mizuse, K. Infrared spectroscopic studies on hydrogen-bonded water networks in gas phase clusters. *Int. Rev. Phys. Chem.* **2013**, 32, 266–307.
- (53) Mizuse, K.; Fujii, A. Structural Origin of the Antimagic Number in Protonated Water Clusters H⁺(H₂O)_n: Spectroscopic Observation of the "Missing" Water Molecule in the Outermost Hydration Shell. *J. Phys. Chem. Lett.* **2011**, *2*, 2130–2134.
- (54) Wang, H.; Agnes, G. R. Kinetically Labile Equilibrium Shifts Induced by the Electrospray Process. *Anal. Chem.* **1999**, *71*, 4166–4172.
- (55) Soleilhac, A.; Dagany, X.; Dugourd, P.; Girod, M.; Antoine, R. Correlating Droplet Size with Temperature Changes in Electrospray Source by Optical Methods. *Anal. Chem.* **2015**, *87*, 8210–8217.